Eur. Phys. J. C (2024) 84:90
https://doi.org/10.1140/epjc/s10052-023-12380-3

THE EUROPEAN PHYSICAL JOURNAL C

Regular Article - Experimental Physics

Measurement of the muon flux at the SND@LHC experiment

R. Albanese[1,2], **A. Alexandrov**[1], **F. Alicante**[1,2], **A. Anokhina**[3], **T. Asada**[1,2], **C. Battilana**[4,5], **A. Bay**[6], **C. Betancourt**[7], **D. Bick**[8], **R. Biswas**[9], **A. Blanco Castro**[10], **V. Boccia**[1,2], **M. Bogomilov**[11], **D. Bonacorsi**[4,5], **W. M. Bonivento**[12], **P. Bordalo**[10], **A. Boyarsky**[13,14], **S. Buontempo**[1], **M. Campanelli**[15], **T. Camporesi**[9], **V. Canale**[1,2], **A. Castro**[4,5], **D. Centanni**[1,16], **F. Cerutti**[9], **M. Chernyavskiy**[3], **K. -Y. Choi**[17], **S. Cholak**[6], **F. Cindolo**[4], **M. Climescu**[18], **A. P. Conaboy**[19], **G. M. Dallavalle**[4], **D. Davino**[1,20], **P. T. de Bryas**[6], **G. De Lellis**[1,2], **M. De Magistris**[1,16], **A. De Roeck**[9], **A. De Rújula**[9], **M. De Serio**[21,22], **D. De Simone**[7], **A. Di Crescenzo**[1,2], **R. Donà**[4,5], **O. Durhan**[23], **F. Fabbri**[4], **F. Fedotovs**[15], **M. Ferrillo**[7], **M. Ferro-Luzzi**[9], **R. A. Fini**[21], **A. Fiorillo**[1,2], **R. Fresa**[1,24], **W. Funk**[9], **F. M. Garay Walls**[25], **A. Golovatiuk**[1,2], **A. Golutvin**[26], **E. Graverini**[6], **A. M. Guler**[23], **V. Guliaeva**[3], **G. J. Haefeli**[6], **C. Hagner**[8], **J. C. Helo Herrera**[27,38], **E. van Herwijnen**[26], **P. Iengo**[1], **S. Ilieva**[1,2,11,a], **A. Infantino**[9], **A. Iuliano**[1,2], **R. Jacobsson**[9], **C. Kamiscioglu**[23,28], **A. M. Kauniskangas**[6], **E. Khalikov**[3], **S. H. Kim**[29], **Y. G. Kim**[30], **G. Klioutchnikov**[9], **M. Komatsu**[31], **N. Konovalova**[3], **S. Kuleshov**[27,32], **H. M. Lacker**[19], **O. Lantwin**[1], **F. Lasagni Manghi**[4], **A. Lauria**[1,2], **K. Y. Lee**[29], **K. S. Lee**[33], **S. Lo Meo**[4], **V. P. Loschiavo**[1,20], **S. Marcellini**[4], **A. Margiotta**[4,5], **A. Mascellani**[6], **A. Miano**[1,2], **A. Mikulenko**[13], **M. C. Montesi**[1,2], **F. L. Navarria**[4,5], **S. Ogawa**[34], **N. Okateva**[3], **M. Ovchynnikov**[13], **G. Paggi**[4,5], **B. D. Park**[29], **A. Pastore**[21], **A. Perrotta**[4], **D. Podgrudkov**[3], **N. Polukhina**[3], **A. Prota**[1,2], **A. Quercia**[1,2], **S. Ramos**[10], **A. Reghunath**[19], **T. Roganova**[3], **F. Ronchetti**[6], **T. Rovelli**[4,5], **O. Ruchayskiy**[35], **T. Ruf**[9], **M. Sabate Gilarte**[9], **Z. Sadykov**[1], **M. Samoilov**[3], **V. Scalera**[1,16], **W. Schmidt-Parzefall**[8], **O. Schneider**[6], **G. Sekhniaidze**[1], **N. Serra**[7], **M. Shaposhnikov**[6], **V. Shevchenko**[3], **T. Shchedrina**[3], **L. Shchutska**[6], **H. Shibuya**[34,36], **S. Simone**[21,22], **G. P. Siroli**[4,5], **G. Sirri**[4], **G. Soares**[10], **J. Y. Sohn**[29], **O. J. Soto Sandoval**[27,38], **M. Spurio**[4,5], **N. Starkov**[3], **I. Timiryasov**[35], **V. Tioukov**[1], **F. Tramontano**[1,2], **C. Trippl**[6], **E. Ursov**[3], **A. Ustyuzhanin**[1,37], **G. Vankova-Kirilova**[11], **V. Verguilov**[11], **N. Viegas Guerreiro Leonardo**[10], **C. Vilela**[10], **C. Visone**[1,2], **R. Wanke**[18], **E. Yaman**[23], **C. Yazici**[23], **C. S. Yoon**[29], **E. Zaffaroni**[6], **J. Zamora Saa**[27,32]

[1] Sezione INFN di Napoli, 80126 Naples, Italy
[2] Università di Napoli "Federico II", 80126 Naples, Italy
[3] Affiliated with an Institute Covered by a Cooperation Agreement with CERN, Geneva, Switzerland
[4] Sezione INFN di Bologna, 40127 Bologna, Italy
[5] Università di Bologna, 40127 Bologna, Italy
[6] Institute of Physics, EPFL, Lausanne 1015, Switzerland
[7] Physik-Institut, UZH, Zürich 8057, Switzerland
[8] Hamburg University, 22761 Hamburg, Germany
[9] European Organization for Nuclear Research (CERN), 1211 Geneva, Switzerland
[10] Laboratory of Instrumentation and Experimental Particle Physics (LIP), 1649-003 Lisbon, Portugal
[11] Faculty of Physics, Sofia University, Sofia 1164, Bulgaria
[12] Università degli Studi di Cagliari, 09124 Cagliari, Italy
[13] University of Leiden, 2300 RA Leiden, The Netherlands
[14] Taras Shevchenko National University of Kyiv, Kyiv 01033, Ukraine
[15] University College London, London WC1E6BT, UK
[16] Università di Napoli Parthenope, 80143 Naples, Italy
[17] Sungkyunkwan University, Suwon-si 16419, Korea
[18] Institut für Physik and PRISMA Cluster of Excellence, 55099 Mainz, Germany
[19] Humboldt-Universität zu Berlin, 12489 Berlin, Germany
[20] Università del Sannio, 82100 Benevento, Italy
[21] Sezione INFN di Bari, 70126 Bari, Italy

Published online: 27 January 2024

[22] Università di Bari, 70126 Bari, Italy
[23] Middle East Technical University (METU), Ankara 06800, Turkey
[24] Università della Basilicata, 85100 Potenza, Italy
[25] Departamento de Física, Pontificia Universidad Católica de Chile, Santiago 4860, Chile
[26] Imperial College London, London SW72AZ, UK
[27] Millennium Institute for Subatomic physics at high energy frontier-SAPHIR, Santiago 7591538, Chile
[28] Ankara University, Ankara 06100, Turkey
[29] Department of Physics Education and RINS, Gyeongsang National University, Jinju 52828, Korea
[30] Gwangju National University of Education, Gwangju 61204, Korea
[31] Nagoya University, Nagoya 464-8602, Japan
[32] Center for Theoretical and Experimental Particle Physics, Facultad de Ciencias Exactas, Universidad Andrès Bello, Fernandez Concha 700, Santiago, Chile
[33] Korea University, Seoul 02841, Korea
[34] Toho University, Chiba 274-8510, Japan
[35] Niels Bohr Institute, Copenhagen 2100, Denmark
[36] Faculty of Engineering, Kanagawa 221-0802, Japan
[37] Constructor University, 28759 Bremen, Germany
[38] Departamento de Fisica, Facultad de Ciencias, Universidad de La Serena, 1200 La Serena, Chile

Received: 10 October 2023 / Accepted: 23 December 2023

Abstract The Scattering and Neutrino Detector at the LHC (SND@LHC) started taking data at the beginning of Run 3 of the LHC. The experiment is designed to perform measurements with neutrinos produced in proton-proton collisions at the LHC in an energy range between 100 GeV and 1 TeV. It covers a previously unexplored pseudo-rapidity range of $7.2 < \eta < 8.4$. The detector is located 480 m downstream of the ATLAS interaction point in the TI18 tunnel. It comprises a veto system, a target consisting of tungsten plates interleaved with nuclear emulsion and scintillating fiber (SciFi) trackers, followed by a muon detector (UpStream, US and DownStream, DS). In this article we report the measurement of the muon flux in three subdetectors: the emulsion, the SciFi trackers and the DownStream Muon detector. The muon flux per integrated luminosity through an $18\times18\,\mathrm{cm}^2$ area in the emulsion is:

$$1.5 \pm 0.1(\mathrm{stat}) \times 10^4\ \mathrm{fb/cm}^2.$$

The muon flux per integrated luminosity through a $31\times31\,\mathrm{cm}^2$ area in the centre of the SciFi is:

$$2.06 \pm 0.01(\mathrm{stat}) \pm 0.12(\mathrm{sys}) \times 10^4\mathrm{fb/cm}^2$$

The muon flux per integrated luminosity through a $52\times52\,\mathrm{cm}^2$ area in the centre of the downstream muon system is:

$$2.35 \pm 0.01(\mathrm{stat}) \pm 0.10(\mathrm{sys}) \times 10^4\ \mathrm{fb/cm}^2$$

The total relative uncertainty of the measurements by the electronic detectors is 6% for the SciFi and 4% for the DS measurement. The Monte Carlo simulation prediction of these fluxes is 20–25% lower than the measured values.

1 Introduction

The SND@LHC detector [1] is designed to perform measurements with high energy neutrinos (100 GeV–1 TeV) produced in proton-proton collisions at the LHC in the forward pseudo-rapidity region $7.2 < \eta < 8.4$. It is a compact, standalone experiment located 480 m away from the ATLAS interaction point (IP1) in the TI18 tunnel, where it is shielded from collision debris by around 100 m of rock and concrete. The signal events for the experiment are neutrino interactions [2] and searches for dark matter scatterings. However, the majority of recorded events consists of muons arriving from the particles produced in proton-proton collisions at IP1. Since these muons are the main source of background for the neutrino search, it was necessary to do a measurement of the muon flux in the SND@LHC detector.

2 Detector

Figure 1 shows the SND@LHC detector. The electronic detectors provide the time stamp of the neutrino interaction, preselect the interaction region while the vertex is reconstructed using tracks in the emulsion. The veto system is used to tag muons and other charged particles entering the detector from the IP1 direction.

[a] e-mail: simona.ilieva.ilieva@cern.ch (corresponding author)

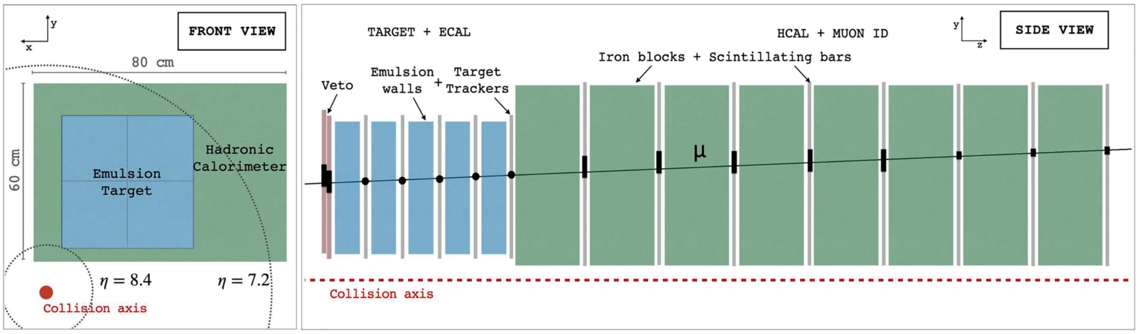

Fig. 1 Schematic layout of the SND@LHC detector. The pseudorapidity η values are the limits for particles hitting the lower left and the upper right corner of the ECC. The side view includes an illustration of a passing-through muon with hits in all subdetectors. For a view of the $x - y$ ranges covered by the SciFi and the muon DS system see Figs. 7 and 8

The veto system comprises two parallel planes of scintillating bars. Each plane consists of seven $1 \times 6 \times 42\,\mathrm{cm}^3$ vertically stacked bars of plastic scintillator.

The target section contains five walls. Each wall consists of four units (‘bricks’) of Emulsion Cloud Chambers (ECC) and is followed by a scintillating fiber (SciFi) station for tracking.

Each SciFi station consists of one horizontal and one vertical $39 \times 39\,\mathrm{cm}^2$ plane. Each plane comprises six staggered layers of 250 µm diameter polystyrene-based scintillating fibers. The single particle spatial resolution in one plane is ∼150 µm and the time resolution for a particle crossing both x and y planes is about 250 ps.

The muon system consists of two parts: the first five stations (UpStream, US), and the last three stations (DownsStream (DS), see Fig. 1). Each US station consists of 10 stacked horizontal scintillator bars of $82.5 \times 6 \times 1\,\mathrm{cm}^3$, resulting in a coarse y view. A DS station consists of two layers of thinner bars measuring $82.5 \times 1 \times 1\,\mathrm{cm}^3$, arranged in alternating x and y planes, allowing for a spatial resolution in each axis of less than 1 cm. The eight scintillator stations are interleaved with 20 cm thick iron blocks. Events with hits in the DS detector and the SciFi tracker are used to identify muons.

A right-handed coordinate system is used, with z along the nominal proton-proton collision axis and pointing away from IP1, x pointing away from the centre of the LHC, and y vertically aligned and pointing upwards.

All signals exceeding preset thresholds are read out by the front-end electronics and clustered in time to form events. A software noise filter is applied to the events online, resulting in negligible detector deadtime and negligible loss in signal efficiency. Events satisfying certain topological criteria, such as the presence of hits in several detector planes, are read out. At the highest instantaneous luminosity in 2022 ($2.5 \times 10^{34}\,\mathrm{cm}^{-2}\,\mathrm{s}^{-1}$) this generated a rate of around 5.4 kHz.

3 Data and Monte Carlo simulations

3.1 Data sample

3.1.1 Emulsion

The data used in the analysis of the emulsion was from a brick that was irradiated during the (LHC commissioning) period 7th May–26th July 2022. The integrated luminosity for this period was 0.5 fb^{-1}.

3.1.2 Electronic detectors

During the production 13.6 TeV proton physics period in 2022 SND@LHC recorded an integrated luminosity of 36.8 fb^{-1}. This amounts to 95% of the total 38.7 fb^{-1} delivered luminosity at IP1, as reported by ATLAS [3]. We used two runs (see Table 1) from this data for the muon flux measurement using the electronic detectors.

3.1.3 Muons not from beams colliding in IP1

For the calculation of the muon flux, we are only interested in the muons that come from pp collisions in IP1. The LHC filling scheme specifies which bunches cross at different interaction points and which bunches of Beam 1 and Beam 2 are circulating in the LHC without colliding.[1] Since the SND@LHC detector is 480 m away from IP1, there is a phase shift between the filling scheme and the SND@LHC event timestamp. The phase adjustments for both beams are determined by finding the maximum overlap with SND@LHC event rates. The synchronized bunch structure then allows us to determine whether an event is associated with a collision at IP1, whether it originates from Beam 1 without colliding in

[1] The clockwise circulating beam is denoted Beam 1, while the counter clockwise circulating beam is denoted Beam 2 [4].

Table 1 List of the two selected SND@LHC 2022 data runs. The runs are chosen to have large event counts, high delivered luminosity, isolated LHC bunches of Beam 2 passing without collisions, and different LHC filling schemes

LHC fill number	Integrated luminosity [fb^{-1}]	Mean number of interactions at IP1 per bunch crossing	SND@LHC run number	Recorded events by SND@LHC [10^6]	Date, year 2022	Duration [h]
8088	0.337	35.2	4705	71	3 Aug	12.5
8297	0.529	45.4	5086	101	20 Oct	19.8

IP1, or whether it originates from Beam 2 without colliding in IP2. For the determination of the muon flux, the latter two contributions have to be subtracted from the total number of recorded muons associated with IP1 collisions [5]. The muon contribution from IP2 collisions is negligible given the small difference in the event rates associated with circulation of non-colliding Beam 2 bunches and IP2 collisions.

3.2 Monte Carlo simulations

The *pp* event generation was done with DPMJET (Dual Parton Model) [6]. The subsequent muon production from the *pp* collisions was simulated with FLUKA [7]. The propagation of collision debris in the LHC towards the SND@LHC detector was done using the LHC FLUKA model [8]. The particle transport was stopped at a 1.8×1.8 m^2 scoring plane, located in the rock about 60 m upstream of SND@LHC. This dataset consists of particles from 200×10^6 *pp* collisions simulated with LHC Run 3 beam conditions.

The propagation of muons from the scoring plane to the detector and their interactions were modelled with a GEANT4 simulation [9] of SND@LHC and its surroundings.

4 Track finding and fitting methods for the electronic detectors

Most muons traveling from IP1 towards SND@LHC leave straight tracks in the detector. Two track-finding methods were implemented in the SND@LHC software framework. One of them makes use of a custom track-finding solution that minimizes the residuals between measured points and a straight-line track candidate, denoted Simple Tracking (ST). The other tracking approach employs the Hough transform [10] pattern recognition method and is referred to as Hough Transform (HT). In both cases, the track fitting is done using the Kalman filter method in the GENFIT package [11].

Since the SciFi and DS detectors have a different granularity and the acceptance of the DS is 2.4 times larger than that of the SciFi, the muon flux is determined independently in these two detector subsystems.

Table 2 SciFi and DS tracking efficiencies for simple and Hough transform tracking methods

System	Tracking algorithm	Tracking efficiency
SciFi	Simple tracking	0.868 ± 0.009
	Hough transform	0.956 ± 0.007
DS	Simple tracking	0.937 ± 0.007
	Hough transform	0.944 ± 0.009

Track building in these subsystems is done separately in the horizontal $x-z$ and vertical $y-z$ plane. The final three dimensional track is built by combining the horizontal and vertical tracks [5].

The tracking efficiency in each detector and for each of the tracking methods is estimated using data (see Table 2). The uncertainty of the efficiency is evaluated as three times the standard deviation of tracking efficiency values over 1×1 cm^2 $x-y$ detector coordinate bins. The HT method has a better efficiency and it is used as the baseline for this analysis.

5 Angular distribution in the electronic detectors

Most muons reaching SND@LHC have tracks with small angles with respect to the z axis, see Figs. 2 and 3. The main peak corresponds to the source at IP1. This peak has large tails due to multiple scattering along the 480 m path from IP1 to SND@LHC. The structures at negative slopes originate from beam-gas interactions. As shown in Fig. 4, after selecting SND@LHC events corresponding to non-colliding Beam 2 bunches and no present bunches of Beam 1 (B2noB1), almost all reconstructed tracks have negative $x-z$ slopes. Track direction studies based on detector hit timing show that particles with reconstructed tracks in such B2noB1 events enter the detector from the back (see Fig. 5). Therefore, the origin of these particles must be downstream of the DS stations.

Figure 6 shows the angles of SciFi tracks in the $x-z$ plane in the range of very small angles ($-0.02<\tan\theta_{xz}<0.02$). The angular distance between the two slightly shifted peaks is about 5 mrad. A similar structure is seen in the emulsion data (see Fig. 10) and the Monte Carlo simulation (see Fig. 14).

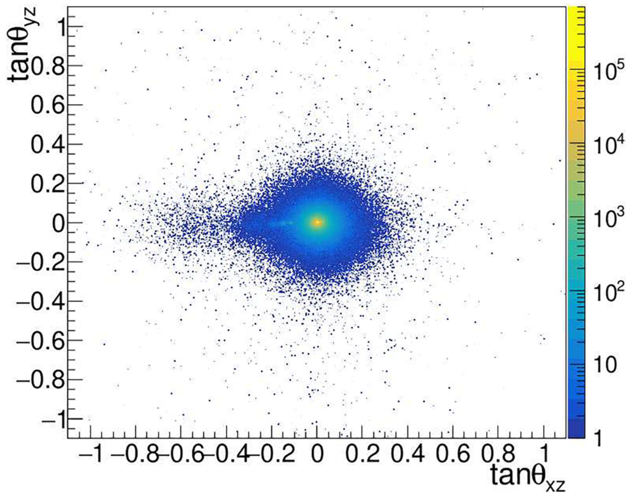

Fig. 2 SciFi track slopes of reconstructed tracks. The slopes in the horizontal $x-z$ plane ($\tan\theta_{\mathrm{xz}}$) and in the vertical $y-z$ plane ($\tan\theta_{\mathrm{yz}}$) are derived from the differences of the track coordinates between the first and the last track point in the detector

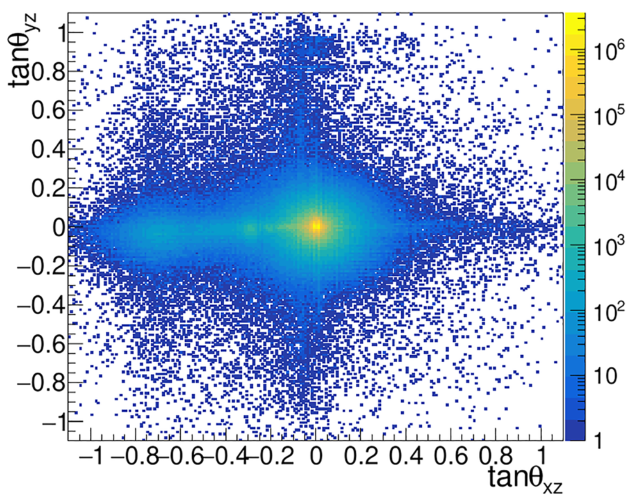

Fig. 3 DS track slopes of reconstructed tracks. The slopes in the horizontal $x-z$ plane ($\tan\theta_{\mathrm{xz}}$) and in the vertical $y-z$ plane ($\tan\theta_{\mathrm{yz}}$) are derived from the differences of the track coordinates between the first and the last track point in the detector

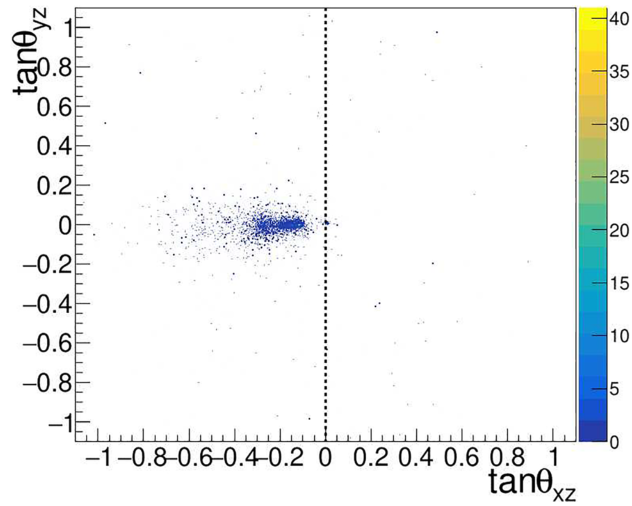

Fig. 4 SciFi track slopes for data events in sync with B2noB1 LHC bunches

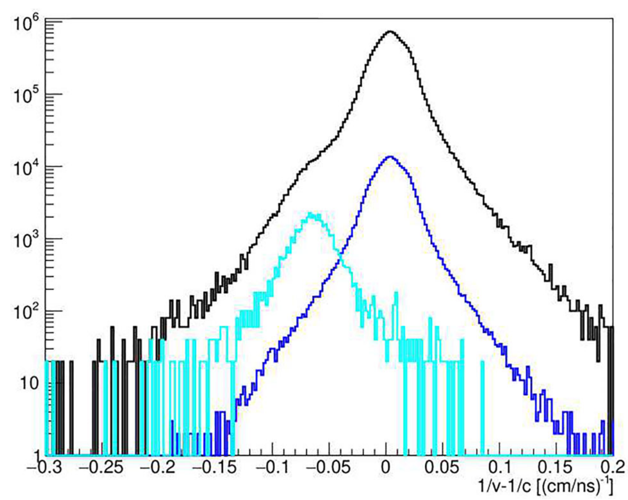

Fig. 5 Track separation by particle propagation direction using SciFi tracks. The black curve corresponds to tracks reconstructed in all events. The blue curve corresponds to tracks in events of non-colliding Beam 1 bunches and no present bunches of Beam 2 (B1noB2). The cyan curve is for events of non-colliding Beam 2 bunches and no present bunches of Beam 1 (B2noB1) bunches. Tracks of particles moving from the DS towards the SciFi (backward going tracks), must have $1/v - 1/c$ values around $-2/c$ or $-$ 0.067 (cm/ns)$^{-1}$. For each track, the value $1/v$ is obtained from a straight line fit to a plot of position difference versus timing difference between each track point and its first upstream point in the SciFi detector

From the FLUKA simulation it is known that muons in the main peak originate at IP1 and muons in the other peak are from particle (pion and kaon) decays at various locations [5].

6 Muon flux in the electronic detectors

The muon flux is defined as the number of reconstructed tracks per corresponding IP1 integrated luminosity and unit detector area. The number of tracks is corrected for the tracking efficiency.

The muon flux in the SciFi and DS detectors is estimated in an area with uniform tracking efficiency [5]. For the SciFi this is the area between $-42\,\mathrm{cm} \le x \le -11\,\mathrm{cm}$ and $18\,\mathrm{cm} \le y \le 49\,\mathrm{cm}$ ($31\times31\,\mathrm{cm}^2$, see Fig. 7). For the DS this is the area between $-54\,\mathrm{cm} \le x \le -2\,\mathrm{cm}$ and $12\,\mathrm{cm} \le y \le 64\,\mathrm{cm}$ ($52\times52\,\mathrm{cm}^2$, see Fig. 8).

6.1 Systematic uncertainties

The Monte Carlo simulation has shown that there are differences in the tracking performance of ST and HT depending

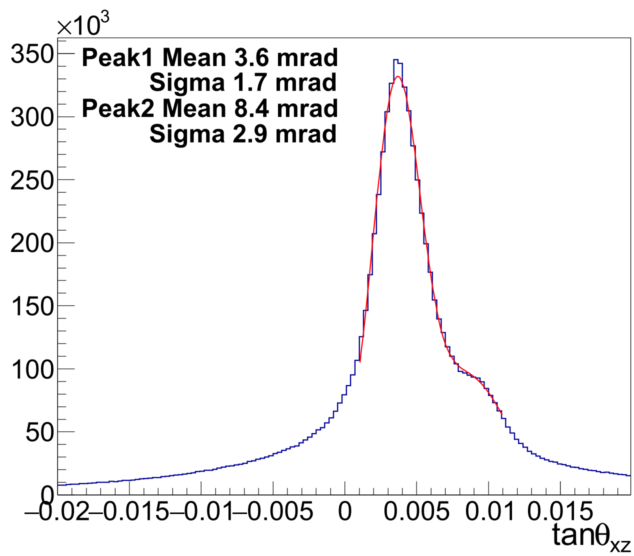

Fig. 6 Angles of SciFi tracks in the $x-z$ plane. The two peaks are fitted with a two Gaussian function

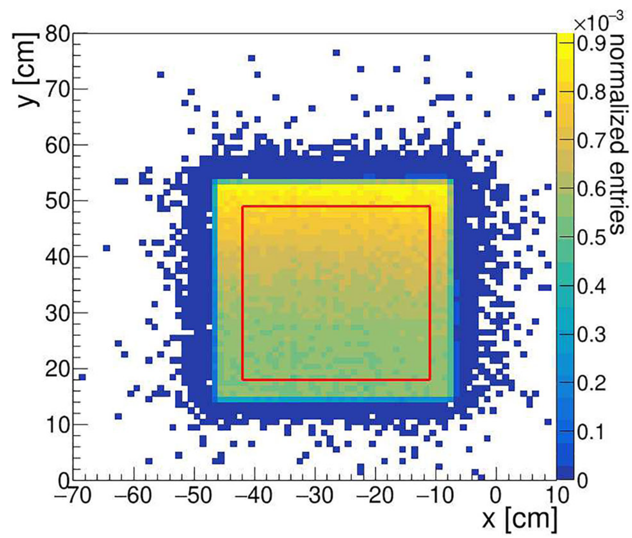

Fig. 7 Distribution of SciFi tracks at the most upstream detector plane. The distribution is normalized to unit integral. The red border delimits the region considered for the SciFi muon flux measurement

on the energy spectrum (20% for SciFi and 10% for DS, see [5]). Because of this dependence, the choice of tracking method introduces a bias in the flux result as it gives preference to muons in certain energy bins. However, the energy spectrum of the data is unknown, and hence the bias can not be determined. For this reason, the difference of the muon fluxes obtained for tracks built with the ST and HT methods is assigned to a systematic uncertainty.

Since the tracking efficiency directly enters the muon flux estimate, its uncertainty is assigned to a systematic uncertainty.

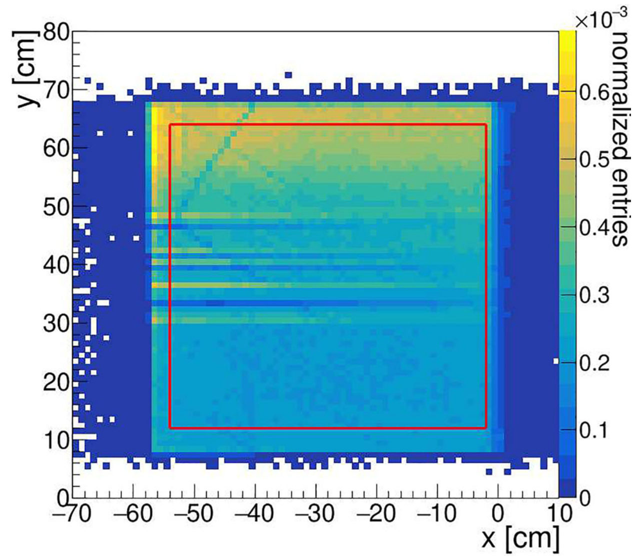

Fig. 8 Distribution of DS tracks at the most upstream detector plane. The distribution is normalized to unit integral. Horizontal stripes of lower counts in the central part of the detector are caused by scintillator bar inefficiencies. The red border delimits the region considered for the DS muon flux measurement

Table 3 Relative magnitude of the sources of systematic uncertainty for the muon flux measurement: luminosity, fluctuations of the tracking efficiency in different $x-y$ detector regions, and the choice of tracking method

System	Luminosity uncertainty [%]	Tracking efficiency [%]	Choice of tracking method [%]
SciFi	2.2	2.2	4.8
DS	2.2	2.9	2.0

The third source of systematic uncertainty is the integrated luminosity for an LHC fill, whose value is used to normalize the muon flux. The ATLAS collaboration reports a 2.2% uncertainty in the integrated luminosity for data recorded in 2022 [3].

The systematic uncertainties per source are given in Table 3 for the SciFi and the DS. For the SciFi the dominant source of uncertainty is the choice of tracking method, while for the DS muon detector it is the tracking efficiency. The total systematic uncertainty is the quadrature sum of the uncertainties for all sources.

6.2 Results

The muon flux per integrated luminosity for SciFi and DS are presented in Table 4, together with the statistical and systematic uncertainties. The DS muon flux is larger than the SciFi flux because of the non-uniform distribution of tracks in the vertical direction (see Figs. 7 and 8) and the difference

Table 4 Muon flux in the SciFi and the DS detectors

System	Muon flux [10^4 fb/cm^2]
SciFi	$2.06 \pm 0.01\,(\text{stat.}) \pm 0.12\,(\text{sys.})$
DS	$2.35 \pm 0.01\,(\text{stat.}) \pm 0.10\,(\text{sys.})$

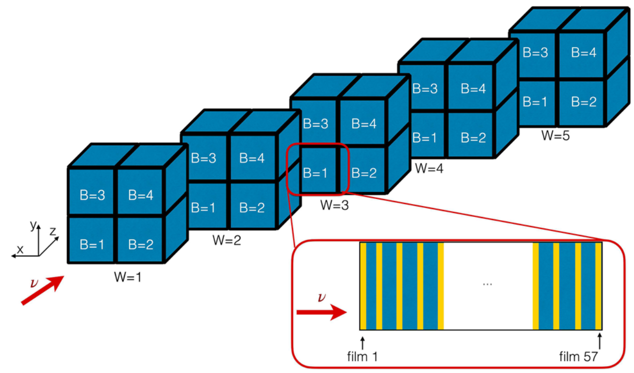

Fig. 9 Layout of the SND@LHC emulsion target. The brick instrumented emulsions is highlighted, showing a layout of its inner structure along its depth

in acceptance. The total relative uncertainty is 6% for the SciFi measurement and 4% for the DS.

7 Muon flux in the emulsion

During the commissioning phase of the LHC, a reduced target was instrumented with a single brick to establish whether the occupancy of the emulsion could be determined, thus providing input for the analysis of future targets.

7.1 Detector layout and track reconstruction

Figure 9 shows the layout of Emulsion Target 0 that took the data used in this analysis. The ECC brick was located in the third wall, in the position closest to the line of sight in the transverse plane.

After development and scanning, the data reconstruction was performed with the FEDRA ROOT C++ library [12]. The films were aligned in the reference system of the ECC brick and the tracks in the emulsion target were reconstructed [13].

7.2 Angular distribution

The angular distribution of the tracks reconstructed in the emulsion is shown in Fig. 10. The presence of a second peak in the $x - z$ component can be seen. Fitting the distribution of the angle in the $x - z$ plane with a two Gaussian function results in a distance between the peaks of ~ 6 mrad. The

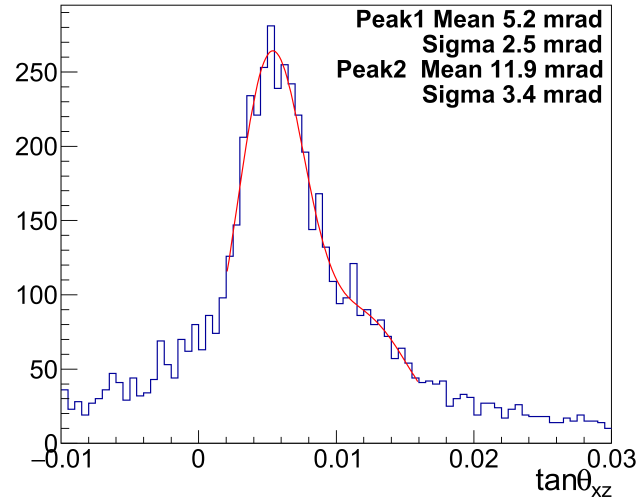

Fig. 10 Angles of emulsion tracks in the $x - z$ plane. The two peaks are fitted with a two Gaussian function

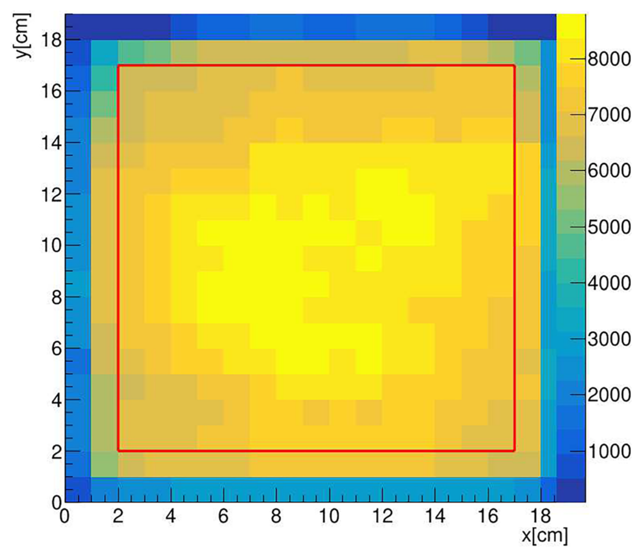

Fig. 11 Distribution of tracks at the most upstream film in each 1cm^2 cell, corrected for reconstruction efficiency. The red border represents the region considered for measuring the average density. The coordinates on the axes are local coordinates on the surface of the brick

angular distribution with two peaks is similar to that observed with the electronic detectors in Fig. 6.

7.3 Results

The spatial density of the reconstructed tracks, after correcting for the tracking efficiency [13], is shown in Fig. 11. In the region represented within the red border, the track density is 7.7 ± 0.6 (stat) $\times\ 10^3$ cm^{-2}. For the luminosity integrated in the emulsion target during the exposure time, the track density corresponds to a muon flux of 1.5 ± 0.1 (stat) $\times\ 10^4$ fb/cm^2.

Table 5 Muon flux in the SciFi and the DS detectors in identical detector areas: $-42\,\text{cm} \le x \le -11\,\text{cm}$ and $18\,\text{cm} \le y \le 49\,\text{cm}$

System	Muon flux [10^4 fb/cm^2] same fiducial area
SciFi	$2.06 \pm 0.01(\text{stat.}) \pm 0.12(\text{sys.})$
DS	$2.02 \pm 0.01(\text{stat.}) \pm 0.08(\text{sys.})$

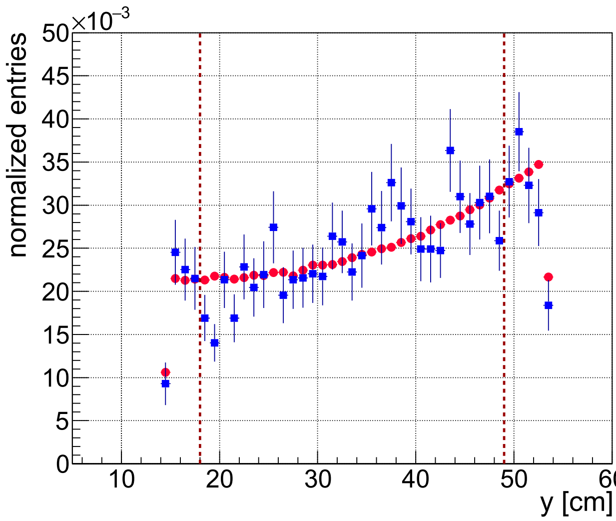

Fig. 12 SciFi tracks in data (red) and Monte Carlo simulation (blue) as a function of y. The dotted red lines indicate the y coordinate boundaries of the detector regions selected for the flux estimation. Each distribution is normalized to unit integral

8 Cross checks

As a cross check of the dependence of the muon flux on the acceptance, the muon flux was also estimated using the SciFi $x-y$ region as acceptance for the electronic subdetectors (see Table 5). In this case, the relative difference between the two measurements is 2%.

The muon flux measured with the SciFi detector is higher than the result obtained from the analysis of the ECC brick (see Sect. 7.2). This is due to the vertical gradient of the flux. In order to perform a reliable comparison, the data from the SciFi in the same region in the transverse plane of the ECC was used for analysis. The resulting muon flux is $1.6 \pm 0.01(\text{stat}) \pm 0.10(\text{sys})\,\text{fb/cm}^2$, consistent with the measurement obtained from emulsion.

9 Monte Carlo simulation expectation

The non-uniform distribution of tracks in the vertical direction in data (see Figs. 7 and 8) is also present in the Monte Carlo simulation (see Figs. 12 and 13). This is due to the complex magnetic field in the LHC. The larger fluctuations in the simulation are due to limited statistics. The few outlier

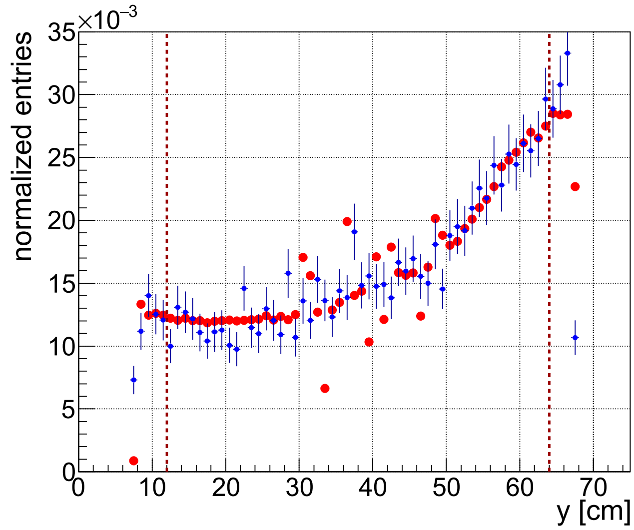

Fig. 13 DS tracks in data (red) and Monte Carlo simulation (blue) as a function of y. The dotted red lines indicate the y coordinate boundaries of the detector regions selected for the flux estimation. Each distribution is normalized to unit integral

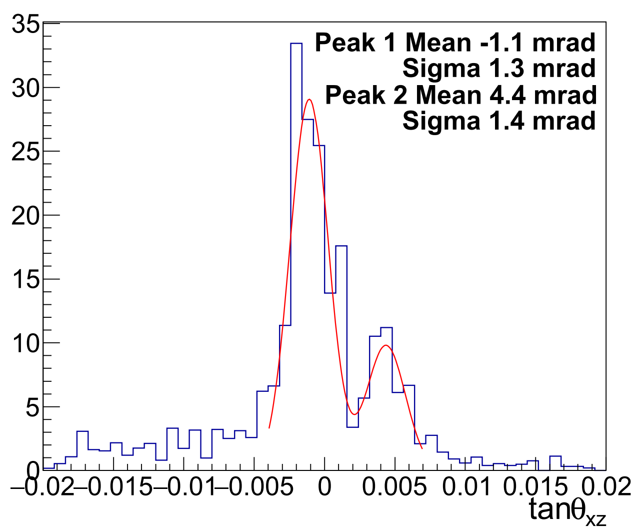

Fig. 14 Simulated SciFi track slopes in the horizontal plane. The region around a few milliradian shows two peaks, which are fitted with a two Gaussian function

data points in the DS (see Fig. 13) are due to inefficient bars (see also Fig. 8).

The two peaks in the angular distribution of the tracks observed in data (see Figs. 6 and 10) are also visible in the MC simulation at a distance of 5.5 mrad (see Fig. 14).

The flux values obtained from the electronic detectors using data are between 20 and 25% larger than those obtained from the Monte Carlo simulation (see Table 6).

There are many physics processes underlying the production of muons from pp collisions, the production of muons

Table 6 Comparison between the muon flux obtained from data and Monte Carlo simulation

System	Sample	Muon flux [10^4 fb/cm^2]	$1 - \frac{\text{sim}}{\text{data}}$ [%]
SciFi	Data	2.06 ± 0.01(stat.) $\pm$ 0.12(sys.)	22 ± 9
	Sim	1.60 ± 0.05(stat.) $\pm$ 0.19(sys.)	
DS	Data	2.35 ± 0.01(stat.) $\pm$ 0.10(sys.)	24 ± 9
	Sim	1.79 ± 0.03(stat.) $\pm$ 0.15(sys.)	

through decays of non-interacting pions and kaons, as well as their transportation through magnetic elements of the LHC and several hundred meters of rock. Given this complexity and the fact that the three stages are simulated with different Monte Carlo programs, each with an associated uncertainty ranging from 10 to 200%, the agreement between the prediction by the Monte Carlo simulation and the measured flux is remarkable.

10 Conclusion

The muon flux at SND@LHC is measured using three independent tracking detectors: ECC, SciFi and the DS. The analyzed data samples were taken during the 2022 LHC proton run. The muon flux per integrated luminosity through an $18 \times 18\,\text{cm}^2$ area of one ECC brick is $1.5 \pm 0.1\,(\text{stat}) \times 10^4\,\text{fb/cm}^2$. The measured muon flux using the SciFi and a $31 \times 31\,\text{cm}^2$ area between $-42\,\text{cm} \leq x \leq -11\,\text{cm}$ and $18\,\text{cm} \leq y \leq 49\,\text{cm}$ is $2.06 \pm 0.01(\text{stat}) \pm 0.12(\text{sys}) \times 10^4\,\text{fb/cm}^2$. With the DS muon detector and a $52 \times 52\,\text{cm}^2$ area, the muon flux is $2.35 \pm 0.01(\text{stat}) \pm 0.10(\text{sys}) \times 10^4\,\text{fb/cm}^2$. The difference between the estimates is due to a vertical gradient of the flux and the different areas of acceptance of SciFi and DS. The total relative uncertainty of the electronic detectors results is 6% for the SciFi and 4% for the DS measurement. When considering the same area of acceptance for SciFi and ECC, or for SciFi and DS, the measured muon fluxes are in good agreement.

Acknowledgements We express our gratitude to our colleagues in the CERN accelerator departments for the excellent performance of the LHC. We thank the technical and administrative staffs at CERN and at other SND@LHC institutes for their contributions to the success of the SND@LHC effort. We acknowledge and express gratitude to our colleagues in the CERN SY-STI team for the fruitful discussions regarding beam losses during LHC operations. In addition, we acknowledge the support for the construction and operation of the SND@LHC detector provided by the following funding agencies: CERN; the Bulgarian Ministry of Education and Science within the National Roadmap for Research Infrastructures 2020-2027 (object CERN); ANID-Millennium Program-ICN2019_044 (Chile); the Deutsche Forschungsgemeinschaft (DFG, ID 496466340); the Italian National Institute for Nuclear Physics (INFN); JSPS, MEXT, the Global COE program of Nagoya University, the Promotion and Mutual Aid Corporation for Private Schools of Japan for Japan; the National Research Foundation of Korea with grant numbers 2021R1A2C2011003, 2020R1A2C1099546, 2021R1F1A1061717, and 2022R1A2C100505; Fundação para a Ciência e a Tecnologia, FCT (Portugal), CERN/FIS-INS/0028/2021; the Swiss National Science Foundation (SNSF); TENMAK for Turkey (Grant No. 2022TENMAK(CERN) A5.H3.F2-1). M. Climesu, H. Lacker and R. Wanke are funded by the Deutsche Forschungsgemeinschaft (DFG, German Research Foundation), Project 496466340. We acknowledge the funding of individuals by Fundação para a Ciência e a Tecnologia, FCT (Portugal) with grant numbers CEECIND/01334/2018, CEECINST/00032/2021 and PRT/BD/153351/2021. We thank Luis Lopes, Jakob Paul Schmidt and Maik Daniels for their help during the construction.

Data Availability Statement This manuscript has no associated data or the data will not be deposited. [Authors' comment: The raw datasets analysed during the current study are available from the corresponding author on reasonable request.]

References

1. G. Acampora et al., SND@LHC - Scattering and Neutrino Detector at the LHC. https://cds.cern.ch/record/2834502, Geneva (2022)
2. R. Albanese, (SND@LHC Collaboration): Observation of collider muon neutrinos with the SND@LHC experiment. Phys. Rev. Lett. **131**, 031802 (2023). https://doi.org/10.1103/PhysRevLett.131.031802
3. Preliminary analysis of the luminosity calibration of the ATLAS 13.6 TeV data recorded in 2022. Technical report, CERN, Geneva (2023). http://cds.cern.ch/record/2853525
4. O. S. Brüning, P. Collier, P. Lebrun, S. Myers, R. Ostojic, J. Poole, P. Proudlock, LHC Design Report. CERN Yellow Reports: Monographs. CERN, Geneva (2004). https://doi.org/10.5170/CERN-2004-003-V-1. https://cds.cern.ch/record/782076
5. S. I. Ilieva, Measurement of the muon flux at SND@LHC (2023). http://cds.cern.ch/record/2859193

6. A. Fedynitch, Cascade equations and hadronic interactions at very high energies. PhD thesis, KIT, Karlsruhe, Dept. Phys. (November 2015). https://doi.org/10.5445/IR/1000055433
7. C. Ahdida et al., New capabilities of the FLUKA multi-purpose code. Front. Phys. **9**, 788253 (2022). https://doi.org/10.3389/fphy.2021.788253
8. D. Prelipcean, K. Biłko, F. Cerutti, A. Ciccotelli, D. Di Francesca, R. García Alía, B. Humann, G. Lerner, D. Ricci, M. Sabaté-Gilarte, Comparison Between Run 2 TID Measurements and FLUKA Simulations in the CERN LHC Tunnel of the Atlas Insertion Region. JACoW IPAC 2022, 732–735 (2022). https://doi.org/10.18429/JACoW-IPAC2022-MOPOMS042. http://cds.cern.ch/record/2839993
9. S. Agostinelli et al., GEANT4: a simulation toolkit. Nucl. Instrum. Meth. A **506**, 250–303 (2003). https://doi.org/10.1016/S0168-9002(03)01368-8
10. P.V.C. Hough, Method and means for recognizing complex patterns. U.S. Patent 30696541962 (1962)
11. C. Höppner, S. Neubert, B. Ketzer, S. Paul, A novel generic framework for track fitting in complex detector systems. Nucl. Instrum. Meth. A **620**(2), 518–525 (2010). https://doi.org/10.1016/j.nima.2010.03.136
12. V. Tyukov, I. Kreslo, Y. Petukhov, G. Sirri, The FEDRA framework for emulsion data reconstruction and analysis in the OPERA experiment. Nucl. Instrum. Meth. A **559**, 103–105 (2006). https://doi.org/10.1016/j.nima.2005.11.214
13. A. Iuliano, Measurement of the muon flux with the emulsion target at SND@LHC (2023). https://cds.cern.ch/record/2868917